A Contact Solver Suitable for Finite Elements

J.H. Schutte, Y.H. Wijnant and A. de Boer
University of Twente, Institute of Mechanics, Processes, and Control - Twente,
Structural Dynamics and Acoustics group,
P.O. Box 217, 7500 AE Enschede, The Netherlands
e-mail: **j.h.schutte@utwente.nl**

Abstract

Road traffic noise is regarded as an environmental problem. The interaction between tyre and road surface, the major noise source, is non-linear and needs to be described in the time domain. Finite elements are used more frequently in tyre/road noise models. However, to compute the vibrations and radiated noise pattern of a profiled tyre rolling on a road, contact models lack either accuracy or the calculation times are high. The Structural Dynamics and Acoustics group of the University of Twente has developed an alternative contact algorithm. The contact condition, which states that there is no overlap between the bodies, is satisfied exactly while iteratively solving the equation of motion. Hence, there is no need for contact elements or contact parameters. The possibility to optimize and speed up the algorithm, using e.g. multigrid, is the major advantage of the new approach. In this paper the contact algorithm is applied to a finite element model. A friction model is applied in a transient calculation and the results are shown. The examples show the performance and possibilities of the algorithm.

1   Introduction

In modern society, traffic noise has become an important issue for mental health. A significant contributor to this noise pollution is tyre/road noise, which is caused by the interaction between tyre and road surface. The noise generating mechanisms have been identified, although there is discussion on the relative importance of these mechanisms. From experiments, it is known that spectra of tyre/road noise display a peak in the range of 500–2000 Hz [8].

In order to predict and reduce tyre/road noise, different mathematical and empirical noise predicting models have been developed during the last decades. The main similarity between the mathematical models is that they can be separated in a tyre vibration model and a sound radiation model. Sound radiation has been modelled analytically by equivalent sources and numerically, by use of (in)finite elements or boundary elements. The tyre vibration models range from analytical models, where the tyre vibrations are modelled by means of a ring [1], shell [10] or plate [5], to numerical models based on finite elements. The finite element-based models use approximations in circumferential direction by e.g. an implementation of the Arbitrary Lagrangian Eulerian approach [6, 2] or by the use of waveguide finite elements [7]. The influence of a realistic tread profile cannot be modelled because of these approximations. This requires a full three dimensional model of the tyre. The current tyre models in the finite element package Abaqus are advanced, i.e. it is possible to analyze treaded tyres. However, for tyre road noise the calculation time is large, since the calculation of frequencies up to 2000 Hz requires a very fine mesh and associated large number of degrees of freedom.

The currently used contact models for tyre/road noise lack either accuracy or calculation speed. At the Structural Dynamics and Acoustics group of the University of Twente an alternative contact algorithm has been developed. A characteristic feature of this algorithm is that, while iteratively solving the equation of mo-

tion, the contact condition, i.e. the condition that there is no overlap between the bodies, is satisfied exactly. Hence, there is no need for contact elements, contact parameters, Lagrange multipliers, or regularization. Another major advantage of the new approach is the possibility to use multigrid methods to speed up the algorithm. In the field of elasto-hydrodynamic lubrication, multigrid and multilevel techniques are used extensively to solve contact problems very fast [12, 13]. The proposed contact algorithm is stable and robust.

The new contact algorithm has been successfully applied in a finite difference formulation, where the tyre was modelled as a flexible ring [14]. In a recent paper, the contact algorithm is applied in a finite element model [9] and frictionless normal contact has been validated with the Hertzian solution. In this paper, frictional contact behaviour is discussed. The numerical model and the contact algorithm are explained in section 2. A number of numerical experiments are presented in section 3.

2 Numerical model

For convenience tyre is modelled using a Lagrangian approach. This can easily be replaced in the future by an updated Lagrangian approach to be able to describe large rotations and large deformations in a more advanced model [11]. In this section the finite element model, the contact model and the contact algorithm are discussed.

2.1 Finite element model

The equation of motion reads

$$\boldsymbol{\nabla} \cdot \boldsymbol{\sigma} + \mathbf{b} = \rho \ddot{\mathbf{u}}, \tag{1}$$

where $\boldsymbol{\sigma}$ is the symmetric Cauchy stress tensor, ρ the density, $\mathbf{b}$ the body forces and $\ddot{\mathbf{u}}$ the acceleration. Constitutive equations are needed to couple the Cauchy stress tensor and the density to the kinematics of the deformation. After integration over an arbitrary volume V, introduction of weight functions $\mathbf{w}$ and application of the divergence theorem, the weak form of equation 1 reads

$$\int_V \mathbf{w} \cdot \rho \ddot{\mathbf{u}} \, dV + \int_V \nabla \mathbf{w} : \boldsymbol{\sigma} \, dV = \int_V \mathbf{w} \cdot \mathbf{b} \, dV + \int_S \mathbf{w} \cdot \mathbf{t} \, dS, \tag{2}$$

where $\mathbf{t} = \boldsymbol{\sigma} \cdot \mathbf{n}$ is the traction vector, $\mathbf{n}$ the outward unit normal vector and S the boundary surface. The problem now is discretized by dividing the domain in a number of elements. For the contact algorithm it is preferable to use linear shape functions. Following the Galerkin approach, the weight functions are chosen equal to the shape functions. Then, the equation of motion can be written as a system of coupled, second order differential equations in time

$$\mathbf{M}\ddot{\mathbf{u}} + \mathbf{C}\dot{\mathbf{u}} + \mathbf{K}\mathbf{u} = \mathbf{f}_{\text{ext}}, \tag{3}$$

where $\mathbf{M}$ is mass matrix, $\mathbf{C}$ the damping matrix, $\mathbf{K}$ the stiffness matrix, $\mathbf{u}$ the nodal displacement vector, and $\mathbf{f}_{\text{ext}} = \mathbf{f}_t + \mathbf{f}_b$ the external force vector; the sum of the nodal body forces and nodal traction forces (see the righthand side of equation 2). Equation 3 can be solved in time when sufficient boundary conditions are applied. As a tyre cannot penetrate the road surface, we search for a solution of equation 3 subject to this geometric constraint. This contact behaviour is described by the contact model in the next section.

2.2 Contact model

Contact for finite elements is frequently studied in literature. For an overview the reader is referred to e.g. [4]. The traction force $\mathbf{f}_t$ working on any surface can be split in a normal pressure component p and tangential friction component $\boldsymbol{\tau}$ according to

$$\mathbf{f}_t = -p\mathbf{n} + \boldsymbol{\tau}, \tag{4}$$

where $\mathbf{n}$ is the outward unit normal. Figure 1 presents the positive directions in the contact model
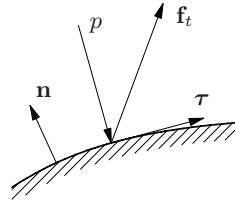
Figure 1: Positive directions in the contact model.

2.2.1 Contact condition

The contact condition is a constraint equation, specifying that the tyre cannot penetrate the road surface. Denoting the distance between the tyre and the road as the 'gap' function g, obviously

$$g \geq 0, \tag{5}$$

where g is the perpendicular distance between a node of the tyre and the contact surface. In contact the gap is equal to $g = 0$. Moreover there is assumed to be no adhesion between the two surfaces in contact, i.e. the contact forces can only be compressive

$$p \geq 0. \tag{6}$$

2.2.2 Friction model

When the tyre is in contact with the road, the friction model determines whether the tyre sticks or slips. Coulomb's friction law states that the tangential traction is limited by the normal traction according to

$$|\boldsymbol{\tau}| \leq \mu|p|, \tag{7}$$

where μ is the friction coefficient. In regions of stick Coulomb states $|\boldsymbol{\tau}| < \mu|p|$, in slip regions $|\boldsymbol{\tau}| = \mu|p|$.

Coulomb's friction model is used in the contact algorithm because of its simplicity and the existence of analytical solutions, but the contact algorithm is not restricted to this friction model. The static friction models, like viscous friction and Stribeck friction, or more advanced dynamic models can be applied as well.

The interaction between tyre and road surface is inherently non-linear, and has to be solved in the time domain. The time domain is discretized and the contact algorithm used describes how equation 3 is solved for every time step. In the next section we will discuss the algorithm in terms of the finite element model.

2.2.3 Contact algorithm

In each step, the contact algorithm uses relaxation to calculate an update for each node individually. The applied algorithm has some similarities with the one used by Wu & Du [15], where nodal displacements are used as well. The working of the contact algorithm can best be explained by the flowchart as given in figure 2. For simplicity, the calculation steps in the algorithm are given for the static case. Consider an arbitrary node i. The algorithm first checks if the node is in contact. For nodes i in contact a nodal force $\mathbf{f}^i$ is calculated which is required to keep the node at that position, according to

$$\mathbf{f}^i = \mathbf{K}^{ij}\mathbf{u}^j, \tag{8}$$

where $\mathbf{f}^i$ and $\mathbf{u}^j$ contain a subset of $\mathbf{f}$ and $\mathbf{u}$ respectively; $\mathbf{K}^{ij}$ is the associated subset of matrix $\mathbf{K}$ $(i < j)$. The length of $\mathbf{f}^i$ equals the number of degrees of freedom of node i. The vector $\mathbf{u}^j$ is a subset of $\mathbf{u}$ with all the entries that are associated with node i. In a one-dimensional system for example, $\mathbf{f}^i$ and $\mathbf{u}^j$ are scalars and $\mathbf{K}^{ij}$ is a vector.
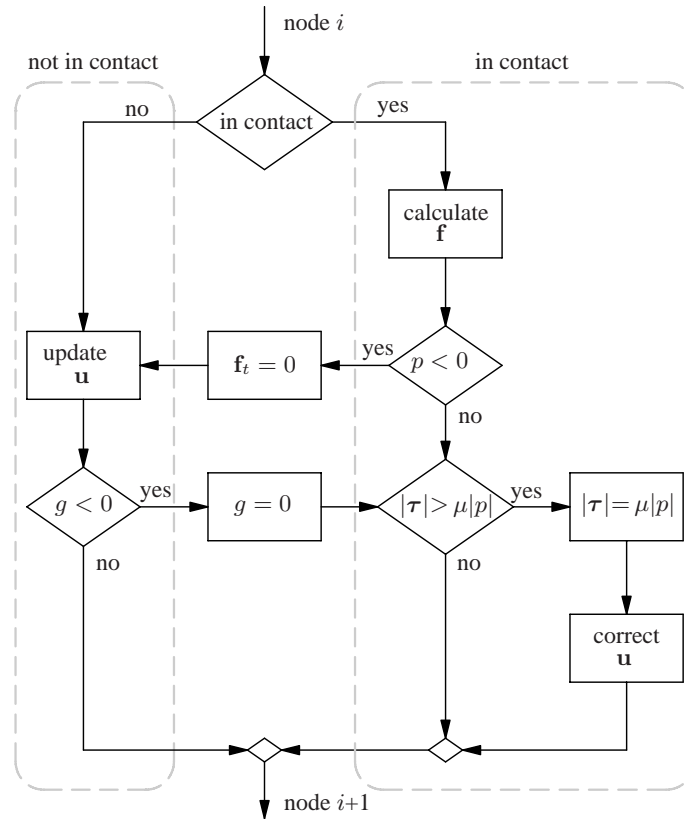
Figure 2: Flowchart of the contact algorithm.

The total external force consists of a body and traction component. The algorithm checks if the pressure p is negative. In case p is positive (tensile), the node is released and the traction force $\mathbf{f}_t$ is set to zero; the node is out of contact. Note that this not necessarily means that $\mathbf{f}^i$ is zero, since body forces can be present. The displacement of the nodes out of contact is updated using Gauss-Seidel relaxation

$$\bar{\mathbf{u}}^i = \tilde{\mathbf{u}}^i + \frac{1}{\mathbf{K}^{ii}} \left(\mathbf{f}^i - \mathbf{K}^{ij} \tilde{\mathbf{u}}^j \right), \tag{9}$$

where $\bar{\mathbf{u}}^i$ is the updated displacement vector of node i, $\tilde{\mathbf{u}}^i$ the original displacement vector of node i, $\mathbf{f}^i$ the nodal external force vector and $\mathbf{K}^{ii}$ is a subset of the stiffness matrix, containing only the entries associated with node i. When a node has been displaced to a point below the surface, the node is in contact and put back on the surface ($g = 0$). Nodes in contact are considered to stick on the surface *a priori*. Equation 7 is used to check whether this assumption is true. If the tangential traction is too high, the friction force is maximal $|\boldsymbol{\tau}| = \mu|p|$. The node slips along the surface ($g = 0$) and the displacement is corrected in tangential direction. In the next step, node $i+1$ is considered and the process continues until convergence has reached for all nodes.

2.3 Time integration

In the previous section, the static case is considered. For dynamic simulations and the implementation of other friction models a discretization in the time domain is necessary. Under appropriate contact conditions, equation 3 is solved in time by a Newmark integration scheme. This implicit second order scheme is commonly used in finite element calculations, because of its consistency, stability and accuracy. In a dynamic calculation the contact algorithm calculates an update for the displacement in the new time step ($\mathbf{u}_{n+1}$). The
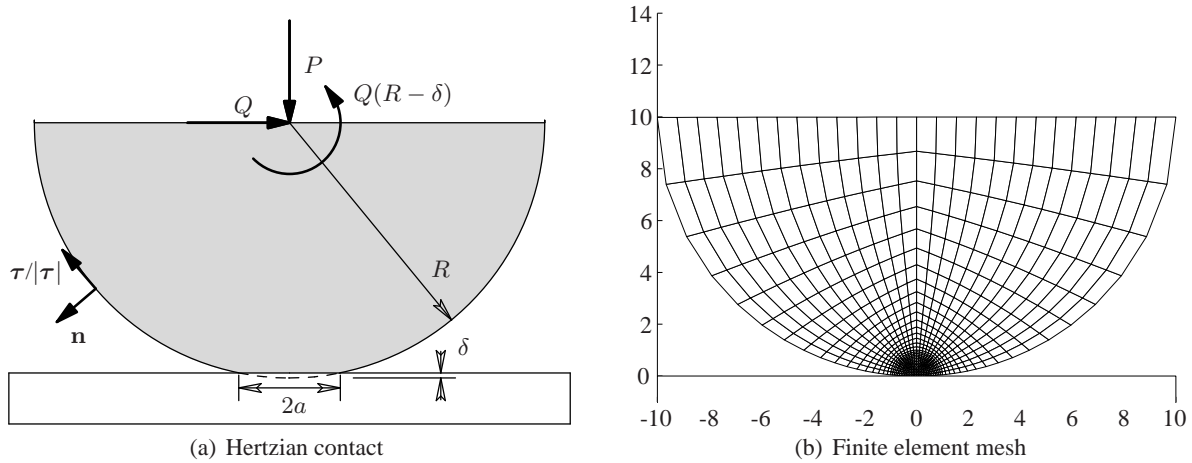
(a) Hertzian contact

(b) Finite element mesh

Figure 3: Hertzian contact by an elastic cylinder on a rigid surface with normal force P and tangential force Q (a) and the undeformed finite element mesh (b).

acceleration and the speed at step $n+1$ follow from the previous time step n and u_{n+1} as

$$\ddot{\mathbf{u}}_{n+1} = \frac{1}{\beta \Delta t^2}\left(\mathbf{u}_{n+1} - \mathbf{u}_n - \Delta t\,\dot{\mathbf{u}}_n\right) - \left(\frac{1}{2\beta} - 1\right)\ddot{\mathbf{u}}_n, \tag{10}$$

$$\dot{\mathbf{u}}_{n+1} = \frac{\gamma}{\beta \Delta t}\left(\mathbf{u}_{n+1} - \mathbf{u}_n\right) - \left(\frac{\gamma}{\beta} - 1\right)\dot{\mathbf{u}}_n - \Delta t\left(\frac{\gamma}{2\beta} - 1\right)\ddot{\mathbf{u}}_n, \tag{11}$$

where Δt is the time step, $\gamma = \frac{1}{2}$ and $\beta = \frac{1}{4}$ for unconditional stability. After the substitution of these relations in equation 3 and application of the initial conditions, $\dot{\mathbf{u}}_{n+1}$ and $\ddot{\mathbf{u}}_{n+1}$ can be solved for each time step. The velocities and accelerations can be used in the friction models.

3 Results

Normal contact has been reviewed in an earlier paper [9], so this paper focusses on tangential loading and friction. Two numerical experiments will be presented in this section, i.e. compression of a cylinder and a bouncing ring. In the two-dimensional finite element simulations the cylinder and ring are modelled using linear elastic material behaviour.

3.1 Loading of a cylinder

The loading of a cylinder on a rigid surface can be a static or a quasi-static problem, depending on the friction model used. It can be solved when the normal and the tangential forces are prescribed (see figure 3).

3.1.1 Normal loading

To test the accuracy of numerical contact a non-trivial test is required for which the analytical solution is available, such as a Hertzian contact [3]. The Hertzian contact formulas describe the contact pressure distribution between two cylinders (line contact) or between two spheres (point contact).

The contact pressure between two cylinders is given by:
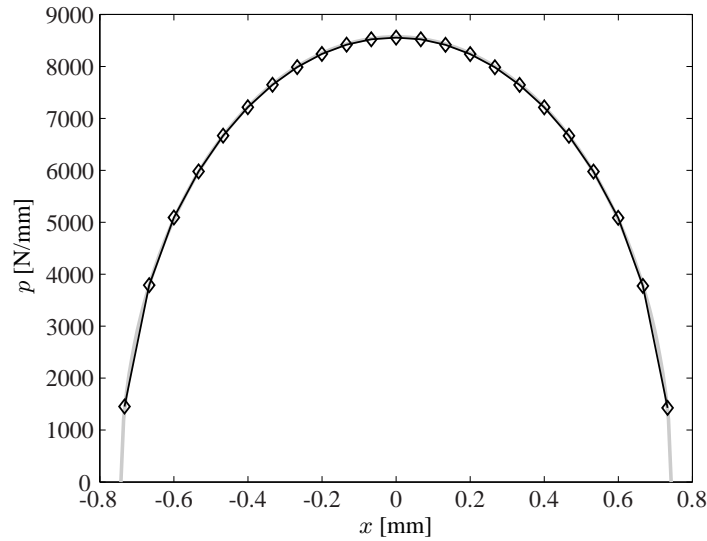
$$p = p_0 \sqrt{1 - x^2/a^2}, \tag{12}$$

Figure 4: Pressure distribution in the contact patch, analytical (—) and numerical solution ($\diamond$).

where p_0 is the maximum pressure, x the Cartesian coordinate along the contact, and a the semi-contact width. For an elastic cylinder on a flat rigid surface the maximum pressure p_0 and semi contact width a are given by

$$p_0 = \sqrt{\frac{PE^*}{\pi R}}, \qquad a = \sqrt{\frac{4PR}{\pi E^*}}, \qquad \text{where} \qquad E^* = \frac{E}{1 - \nu^2}, \tag{13}$$

where P is the normal load per unit length, E^* the effective Young's modulus and R the radius of the cylinder. A numerical simulation is performed with the subsequent parameters: radius $R = 10$ mm, Young's modulus $E = 210 \cdot 10^3$ MPa, Poisson's ratio 0.3, a normal load per unit length $P = 1.0 \cdot 10^4$ N/mm and $Q = 0$. From equation 13 an analytical solution can be derived: maximum pressure $p_0 = 8571$ N/mm and semi-contact width $a = 0.7428$ mm.

The lower half of the cylinder is modelled with 760 bilinear quadrilaterals and compressed on a rigid surface, which both can be considered as half-spaces, as given in figure 3. For a frictionless contact ($\mu = 0$), the numerically and analytically derived contact pressure is depicted in figure 4. The numerical simulations show a good correspondences to the Hertzian contact, with $p_0 = 8555$ N/mm and $0.73 < a < 0.80$ mm ($a = 0.75$ mm after interpolation). The numerical solution converges to the analytical solution. Hence, the contact algorithm is able to predict normal contact pressures in frictionless contact correctly.

In the next example friction is introduced, so the final solution becomes path dependent. The cylinder is compressed by an increasing normal force in 10 equidistant steps on a rigid surface with Coulomb friction ($P = 1.0 \cdot 10^4$ N/mm, $\mu = 0.5$). The resulting stress distribution in the contact patch is given in figure 5, where the direction of τ corresponds to figure 3. The results are according to expectations, i.e. the peak in the normal stress is somewhat higher and the contact width is slightly smaller compared to a frictionless Hertzian contact. The shear stresses causes local slip (microslip) at the borders of the contact patch [3]. The slip direction is opposite to the shear forces working on the cylinder.

3.1.2 Tangential loading

The introduction of a tangential force Q, see figure 3, can increase the region where (micro)slip occurs, and can lead to motion between the cylinder and the surface. For the relative motion between two bodies in contact, a distinction has been made between sliding and rolling. In a situation where cylinders are in contact
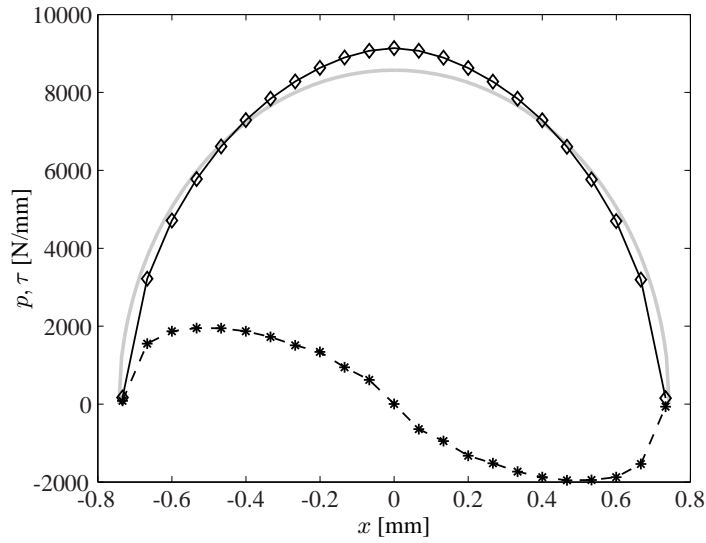
Figure 5: Stress distribution in the contact patch, p ($\diamond$) and τ ($*$) for $\mu = 0.5$, compared to the Hertzian theory $\mu = 0$ (—).

and partial slip occurs, the shear stress in the contact patch can be described by [3].

$$
\boldsymbol{\tau} = \begin{cases} \mu p_0 \left(\sqrt{a^2 - x^2} \right) / a, & c \leq |x| \leq a \quad \text{slip} \\ \mu p_0 \left(\sqrt{a^2 - x^2} - \sqrt{c^2 - x^2} \right) / a, & 0 \leq |x| \leq c \quad \text{stick}, \end{cases} \tag{14}
$$

where

$$
c = a \sqrt{1 - \frac{Q}{\mu P}}. \tag{15}
$$

To prevent a sliding motion between the two cylinders, $Q < \mu P$ and successively $c < a$. So, the sticking region is located in the centre of the contact patch (see figure 6). Total sliding exists when $Q > \mu P$ which induces a relative velocity between the bodies in contact without rotation. Contrary, rolling is the relative angular velocity between two contacting bodies [3]. In case of tractive rolling of elastic cylinders, the stick region moves towards the leading edge of the contact patch. At the trailing edge, slip occurs (see figure 7).

In the numerical simulations, the tangential force $Q = 0.75\mu P$ is applied to the cylinder, whereas all the other parameters remain unchanged. The size of the stick zone $c = 0.5a$. Two load scenarios are considered:

1. *Subsequent loading*. The normal force P is increased in 10 steps; after that the tangential force Q is increased in 10 steps. This scenario is similar to a cylinder which is on the point of slipping.

2. *Initial loading*. In 10 steps the forces P and Q are increased simultaneously until the final load is reached. This scenario is similar to a cylinder which is on the point of rotation.

The results of the first case are given in figure 6. The analytical solution for a completely sliding contact is given as a reference. The numerical results differ from the analytical solution of a sliding cylinder, because the cylinder has rolled over and the stick area is moved towards the leading edge (right). This can be explained by the mesh distortion due to the tangential load. In the Hertzian theory it is assumed that the contact area and pressure distribution are not influenced by the tangential load. The results of the second case are given in figure 7. The analytical solution for a rolling contact between two cylinders is given as a reference. When load P and Q are applied at the same time, the sticking zone moves towards the leading edge. The influence of the tangential load on the contact pressure, explains the differences between the numerical and the analytical solution.

Hence, normal loading is described correctly, tangential loading results in combinations of finite rolling and slip. The contact algorithm converges to the final solution. In the subsequent section a transient dynamic analysis is presented.

3.2 Bouncing ring

To validate the contact algorithm in a dynamic analysis and to evaluate the influence of friction, an elastic ring is considered. It is launched horizontally and due to gravity the ring will bounce on a rigid surface, as depicted in figure 8. The ring has an outer radius of 0.5 m and an inner radius of 0.2 m. At the initial time step ($t = 0$ s), point A is located $h = 0.5$ m above the surface and the ring moves with a constant speed of 10 m/s in positive x-direction. The other parameters are: Young's modulus $E = 1000$ Pa, Poisson's ratio $\nu = 0.3$, the density $\rho = 1.0$ kg/m^3, and gravitational constant $g_0 = 9.81$ m/s^2. After startup, one second of the ring's movement is simulated with a time step $\Delta t = 0.01$ s. Within the total period the ring has touched the surface twice. As in the previous section, Coulomb's friction model is applied with $\mu = 0$ and $\mu = 0.1$.

In figure 8 the first two bounces of the ring on the surface are shown by a series of snap shots. For point A, which is located on the bottom of the ring, the displacement u_y, velocity $\dot{u}_y$ and nodal force f_y are plotted as a function of time. Concerning the time it takes for point A to touch the surface, the numerical solution is similar to the analytical solution $t = \sqrt{2h/g} = 0.32$ s. In the period of contact the velocity of A is zero and the nodal force is positive (compressive on the ring). The contact induces vibrations of the ring, which explains the lower height of the ring at the second bounce. The influence of friction is shown in figure 9, where $\mu = 0.1$. In the contact zone a friction force is acting in the negative x-direction, which induces a rotation in the ring. As a result of the rotation the ring bounces earlier compared to the frictionless case. The current Lagrangian finite element model is not able to model large rotations correctly. In the tyre/road contact model an advanced finite element model will be used to model large deformations [11]. The simulations of the horizontal launch illustrate the working of the contact algorithm in dynamic cases, with slip and small rotations. Although the dynamic results look promising, experimental validation is needed and is in progress.

4 Conclusions

The new contact algorithm, in which the contact condition is satisfied exactly, is applied in a two-dimensional finite element formulation. The algorithm is robust and stable and converges to the correct solution, without the use of contact elements or contact parameters. Another major advantage of the new approach is the possibility to speed up the algorithm by using multigrid. The application of multigrid within the finite element formulation is necessary because of the large calculation times at high frequencies. The description of frictionless and frictional contact behaviour is validated by numerical simulations of a Hertzian contact. Normal and tangential loading are considered with a Coulomb friction model. The application is not limited to static cases only, since the algorithm is successfully applied in a dynamic simulation. In the future, multigrid will be coupled to finite elements and anisotropic material behaviour will be added. The final goal is to compute the vibrations and radiated noise pattern of a profiled tyre rolling on a road.
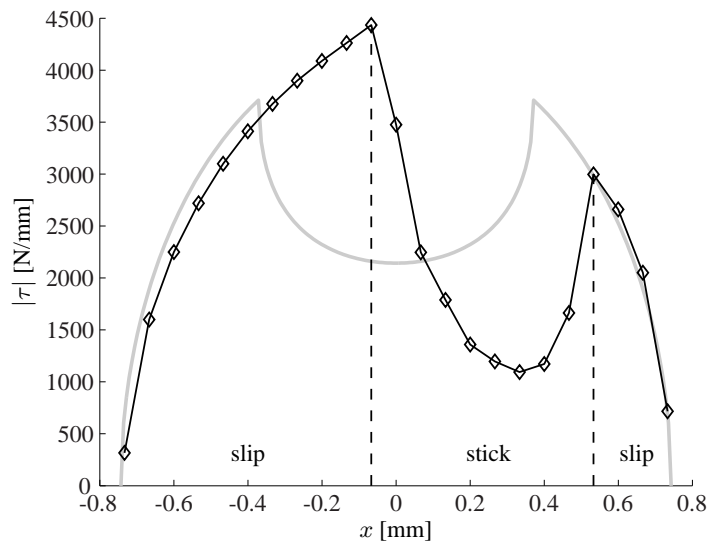
Acknowledgements

Figure 6: Shear stress in the contact patch, numerical results in scenario 1, subsequent loading ($\diamond$). The analytical solution for a sliding contact of a cylinder is given as a reference (——).
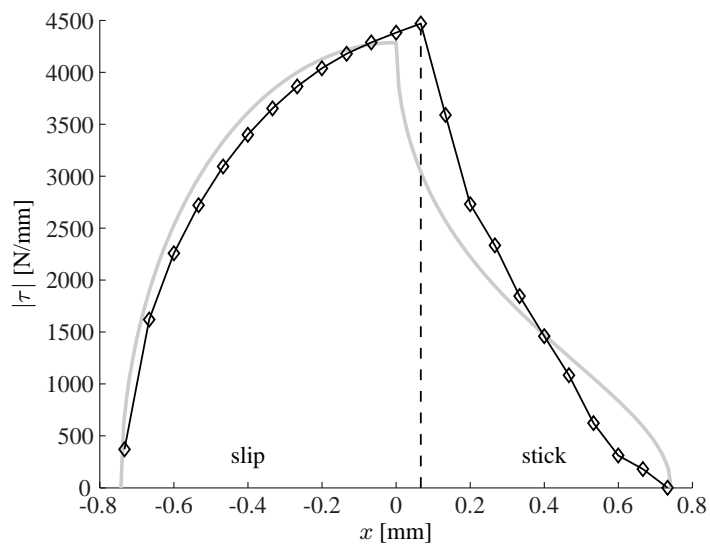

Figure 7: Shear stress in the contact patch, numerical results in scenario 2, initial loading ($\diamond$). The analytical solution for a rolling contact between two cylinders is given as a reference (——).
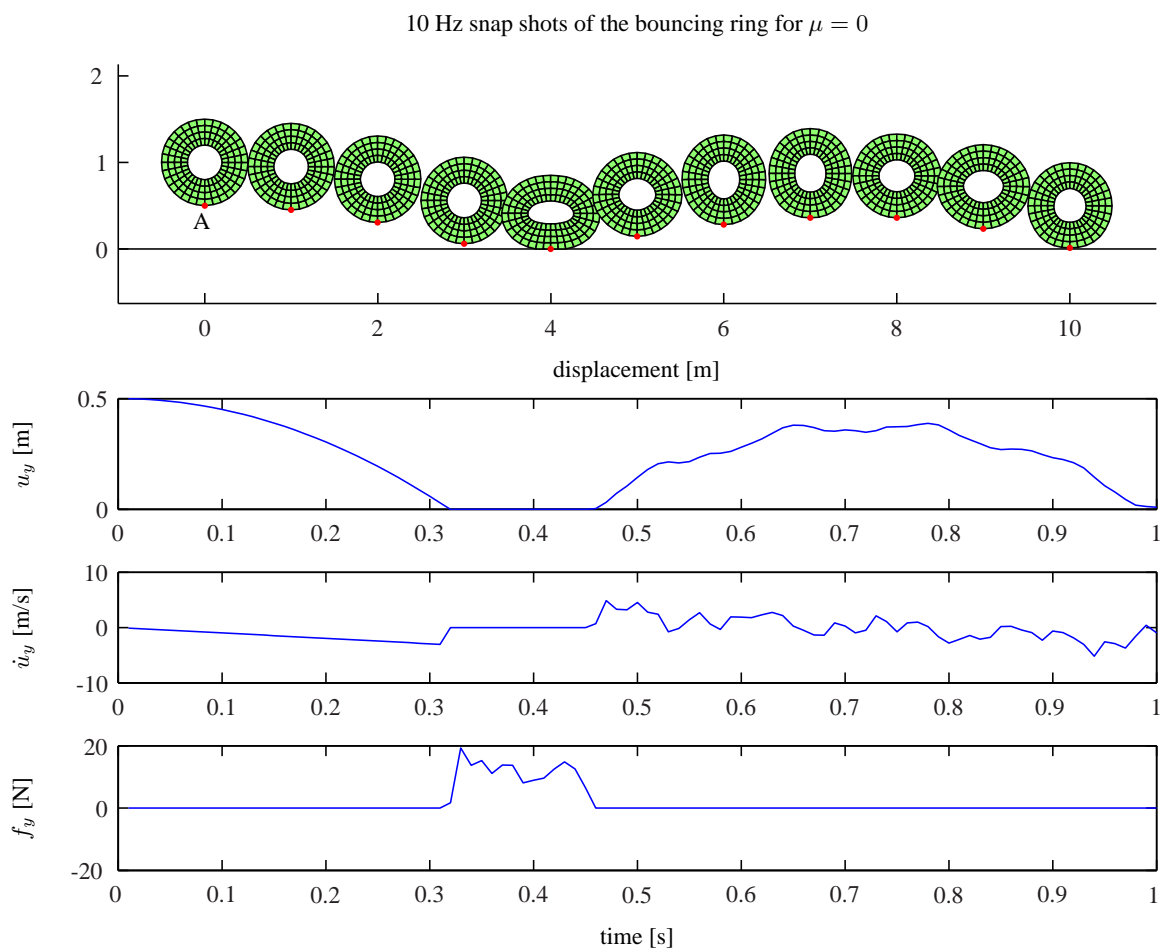
Figure 8: Bouncing ring on a rigid surface at different time steps for $\mu = 0$; displacement u_y, velocity $\dot{u}_y$ and nodal force f_y as a function of time t of point A.
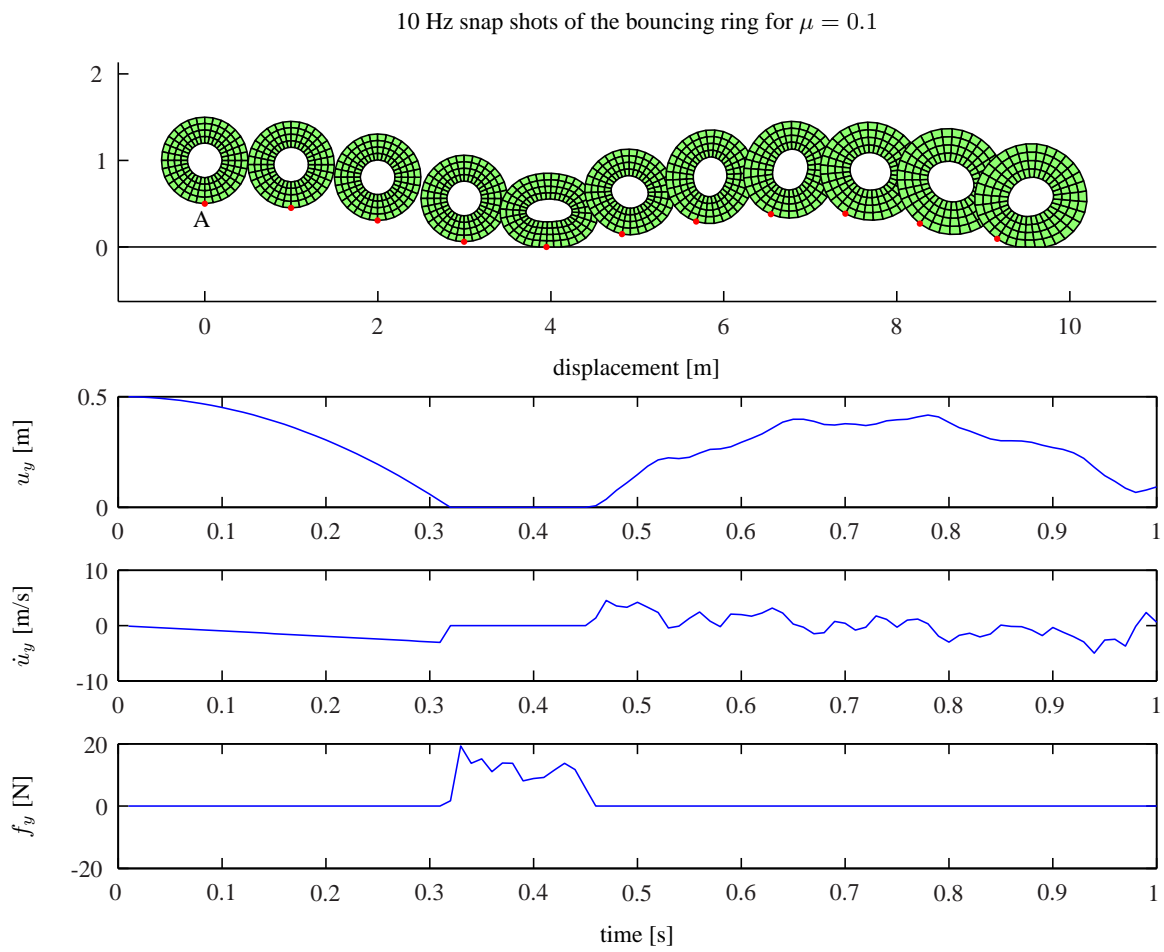
Figure 9: Bouncing ring on a rigid surface at different time steps for $\mu = 0.1$; displacement u_y, velocity $\dot{u}_y$ and nodal force f_y as a function of time t of point A.

References

[1] F. Böhm. Mechanik des Gürtelreifens. *Ingenieur Archiv*, 32(2):82–101, 1966.

[2] M. Brinkmeier, U. Nackenhorst, and M. Ziefle. Finite element analysis of rolling tires – A state of the art review. In *Proceedings of International CTI Conference Automotive Tire Technology*, Stuttgart, Germany, 2007.

[3] K.L. Johnson. *Contact Mechanics*. Cambridge University Press, UK, 1985.

[4] G. Kloosterman. *Contact Methods in Finite Element Simulations*. PhD thesis, University of Twente, Enschede, The Netherlands, 2002.

[5] W. Kropp. *Ein Modell zur Beschreibung des Rollgeräusches eines unprofilierten Gürtelreifens auf rauher Strassenoberfläche*. PhD thesis, Institut für Technische Akustik, Berlin, Germany, 1992.

[6] U. Nackenhorst. The ALE-formulation of bodies in rolling contact – theoretical foundations and finite element approach. *Computer Methods in Applied Mechanics and Engineering*, 193:4299–4322, 2004.

[7] C.-M. Nilsson. *Waveguide finite elements applied on a car tyre*. PhD thesis, Royal Institute of Technology, Stockholm, Sweden, 2004.

[8] U. Sandberg and J.A. Ejsmont. *Tyre/Road Noise Reference Book*. INFORMEX, Harg, SE-59040 Kisa, Sweden, 2002.

[9] J.H. Schutte, Y.H. Wijnant, and A. de Boer. A contact solver suitable for tyre/road noise analysis. In *Proceedings of Acoustics'08*, Paris, France, 2008.

[10] W. Soedel. On the dynamic response of rolling tires according to thin shell approximations. *Journal of Sound and Vibration*, 41(2):233–246, 1975.

[11] R.H.W. ten Thije. *Finite Element Simulations of Laminated Composite Forming Processes*. PhD thesis, University of Twente, Enschede, The Netherlands, 2007.

[12] C.H. Venner. *Multilevel solvers for the EHL line and point contact problems*. PhD thesis, University of Twente, Enschede, The Netherlands, 1991.

[13] Y.H. Wijnant. *Contact Dynamics in the field of Elastohydrodynamic Lubrication*. PhD thesis, University of Twente, Enschede, The Netherlands, 1998.

[14] Y.H. Wijnant and A. de Boer. A new approach to model tyre/road contact. In *Proceedings of ISMA2006*, Leuven, Belgium, 2006.

[15] B. Wu and X. Du. Finite element formulation of radial tires with variable constraint conditions. *Computers and Structures*, 55(5):871–875, 1995.